Molecular Dynamics in Poly(ethene-*alt*-*N*-alkylmaleimide)s As Studied by Broadband Dielectric Spectroscopy

Julius Tsuwi,[†] Dietmar Appelhans,[‡] Stefan Zschoche,[‡] Peter Friedel,[‡] and Friedrich Kremer*,[†]

Institute for Experimental Physics I, University of Leipzig, Linnéstrasse 5, 04103 Leipzig, Germany, and Institute of Polymer Research Dresden, Hohe Strasse 6, 01069 Dresden, Germany

Received March 31, 2004; Revised Manuscript Received May 30, 2004

ABSTRACT: Broadband dielectric spectroscopy has been used to analyze the molecular dynamics in a set of nine poly(ethene-*alt*-*N*-alkylmaleimide)s. The polymers were studied in the frequency range from 0.1 Hz to 10 MHz and at temperatures between 120 and 500 K. The alternating maleimide copolymers possess alkyl side chains varying in length from methyl to octadecyl. Four relaxation processes are observed: (i) a (secondary) β-relaxation corresponding to librational fluctuations of the terminal end group of the alkyl side chain, (ii) the α'-relaxation being assigned to a relaxation of the side chain, (iii) the dynamic glass transition (α-relaxation), being designated to motions of the succinimide ring, and (iv) the α_s-relaxation reflecting cooperative fluctuations of an ensemble of about 2−3 maleimide rings in an underlying helical superstructure. This model is supported by calorimetric measurements and published nuclear magnetic resonance data.

Introduction

A great variety of alternating maleimide (MI) copolymers have been exploited in material sciences in order to improve bulk and surface properties.[1−10] The easy approach, realized by polymer analogous reaction of alternating maleic anhydride copolymers with amino-functionalized compounds, is responsible for the introduction of different side groups with desired characteristic features for their use in special application fields. Especially, the development of MI copolymers for surface engineering is challenged to realize different states of hydrophilic/hydrophobic surface properties[5,7] to be used as top-coat layer, adhesion promoter, or biocompatible layer. It is desirable to combine valuable properties of the side chain and polymer backbone to realize materials that meet specific needs. For this purpose, knowledge of the mechanical and thermal features of MI copolymers[11] is important to enable tailor material properties for surface engineering purposes.

In this paper, broadband dielectric spectroscopy was employed to study the molecular dynamics in poly(ethene-*alt*-*N*-alkylmaleimide)s with varied lengths of *N*-alkyl side chains (Figure 1 and Table 1). It is expected that molecular motions related to main chain and effects arising from the *N*-alkyl side chain can be well understood due to the simplified structures of the side chains. Few dielectric studies on relaxation processes in MI homopolymers[12,13] and copolymers[14] have been reported. The gained dielectric properties in detail build the basis to extend investigations on other MI backbones (styrene−maleimide and octadecene−maleimide combination of the alternating backbone) with different attached side chains for designing hydrophilic/hydrophobic states.[5,11] In general, a better understanding of the molecular dynamics in alternating MI copolymers for the application in surface engineering and for emergence of new uses of these materials can be established.

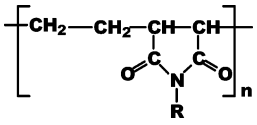

Figure 1. Schematic representation of the chemical formula of the maleimide unit that forms the basis of the main chain. The chemical structure of R is described in Table 1.

Table 1. Abbreviation of the Alternating MI Copolymers and Their Chemical Structure, Molecular Weight (M_w) of the Repeating Unit Ethene−*N*-Alkylmaleimide (RU), and the Calculated Molecular Weight for Nearly 100 % of Converted Maleic Anhydride Groups in Poly(ethene-*alt*-maleic anhydride)

copolymer[a]	side chain attached at R as in Figure 1	M_w of RU [g/mol]	M_w [$\times 10^3$ g/mol]
MI1	CH_3	139.2	∼138
MI2	CH_2-CH_3	153.2	∼152
MI3	$(CH_2)_2-CH_3$	167.2	∼166
MI4	$(CH_2)_3-CH_3$	181.2	∼180
MI6	$(CH_2)_5-CH_3$	209.3	∼207
MI12	$(CH_2)_{11}-CH_3$	293.5	∼291
MI14	$(CH_2)_{13}-CH_3$	321.5	∼319
MI16	$(CH_2)_{15}-CH_3$	349.6	∼347
MI18	$(CH_2)_{17}-CH_3$	377.6	∼374

[a] Degree of polymerization ∼ 992 for the repeating unit ethene−maleic anhydride in converted poly(ethene-*alt*-maleic anhydride).

Experimental Section

Synthesis and Characterization of MI Copolymers. The chemicals [tetrahydrofuran (THF), methylamine, ethylamine, *n*-propylamine, *n*-butylamine, *n*-hexylamine, *n*-dodecylamine, *n*-tetradecylamine, *n*-hexadecylamine, and *n*-octadecylamine] were purchased from Aldrich and used as received. The alternating maleic anhydride (MA) copolymer poly(ethene-*alt*-maleic anhydride) (M_w 125 000 g/mol) was also purchased from Aldrich (Munich, Germany). MI copolymers [MI1, MI2, MI3, MI4, MI6, MI12, MI14, MI16, and MI18] were prepared by dissolving poly(ethene-*alt*-maleic anhydride) (1 mol) and the corresponding amine (1.05 mol) in THF and stirred at 393.15 K for 24 h in an autoclave. The cooled reaction solution was poured into acidic water solution. The resulting MI copolymers were washed intensively with water and then dried in a vacuum at 313 K. The copolymers were character-

[†] University of Leipzig.
[‡] Institute of Polymer Research Dresden.
* To whom correspondence should be addressed. E-mail Kremer@physik.uni-leipzig.de.

10.1021/ma049370o CCC: $27.50
Published on Web 07/07/2004

Table 2. Transition Temperatures and Enthalpies of MI Copolymers Determined by DSC[a]

copolymer	T_g [K]	T_m [K]	ΔH_m [J/g]
MI1	414.3		
MI2	382.4		
MI3	363.5		
MI4	341.0		
MI6	314.6		
MI12	326.9	236.1	10.9
		358.0	3.7
MI14	335.5	266.9	28.5
		367.7	3.9
MI16	338.7	293.0	32.7
		371.0	2.7
MI18	340.2	310.0	45.9
		369.2	1.8

[a] Data were obtained from second heating run at scanning rate = 20 K/min.

ized by attenuated total reflection infrared spectroscopy (ATR-IR), which showed complete conversion of the maleic anhydride ring into the maleimide ring. The ATR-IR spectra did not show additional carbonyl bands of nonconverted maleic anhydride or free acid groups coming from nonconverted and hydrolyzed maleic anhydride groups. NMR investigation of the aliphatic MI did not reveal acid groups, too. Therefore, a nearly complete conversion of the MA units took place. The calculated molecular weights based on the molecular weight of the repeating unit and the average degree of polymerization of the repeating units are shown in Table 1. The complete reaction procedure is similar to the one described in ref 5b.

Glass transition temperatures (T_g) and melting temperatures (T_m) were determined on a differential scanning calorimeter (DSC) Q 1000 with an autosampler (TA Instruments) in the temperature interval 193.15−473.15 K at a heating rate of ±20 K/min. The T_g's were determined using the half-step method from the second heating run (Table 2).

Molecular Modeling. The molecular modeling calculations were carried out on a LINUX operating system, SuSE Distribution 8.2,[15] Kernel 2.4. The geometry and the conformation of the monomer units were optimized by means of quantum mechanical ab initio calculations using GAMESS[16] software by applying a 6-31G** (with diffuse orbitals: for H as +2p and for C, N, O, and F as +3s and +3p) basis set of the Hartree−Fock self-consistent-field method. Single polymer chain models were generated by RESMAIN[17] software, which is able to link up different kinds of monomer units. The formation of connecting monomers of ethene and maleimides for the dipole moment calculation were carried out by an alternating polymerization based on a randomly chosen rotation angle of ±20°. Dipole moment calculations were done using all coordinates of atoms of the current polymer conformation and the relative atomic charges obtained from the quantum mechanical ab initio calculations.

Dielectric Measurements and Data Analysis. To prepare the samples, MI materials were heated in a vacuum until they melted and kept between two brass electrodes (diameter: 10 mm) with 50 μm glass fiber spacers. Isothermal dielectric measurements were performed in the frequency range from 10^{-1} to 10^{7} Hz using a high-resolution dielectric Alpha-analyzer (Novocontrol GmbH). Dielectric spectra were obtained starting from the highest temperature for the range 120−500 K in steps of 2 K. The sample temperature was controlled by a gas heating system based on evaporation of liquid nitrogen (Quatro, Novocontrol GmbH) with a precision of ±0.02 K. Details of the set up are found in ref 18.

For quantitative analysis, the dielectric loss ϵ'' was fitted to a superposition of a conductivity contribution with one or two relaxation functions according to Havriliak and Negami.[19]

$$\epsilon''(\omega) = \frac{\sigma_0}{\epsilon_0}\frac{a}{\omega^s} + \mathrm{Im}\left[\frac{\Delta\epsilon}{[1+(i\omega\tau)^\beta]^\gamma}\right] \qquad (1)$$

The first part on the right-hand side of the equation describes the conductivity while the second part that is added is the imaginary part of the total dielectric loss. In this notation, one relaxation process is assumed. ϵ_0 is the permittivity of free space, and σ_0 is the direct current (dc) conductivity. β and γ are dimensionless parameters describing the symmetric and asymmetric broadening of the distribution of relaxation times, respectively, with $0 < (\beta, \beta\gamma) \leq 1$. For $\beta = \gamma = 1$, eq 1 coincides with an ideal Debye relaxation. The exponent s equals one for Ohmic behavior, deviations ($s < 1$) are caused by electrode polarization or Maxwell−Wagner polarization effects, and a is a factor having the dimensions $[a] = (\mathrm{Hz})^{1-s}$ for $s \neq 1$. From the fits according to eq 1 the relaxation rate $1/\tau_{max}$ can be deduced, which is given at the frequency of maximum dielectric loss ϵ'' for a certain temperature. Within experimental uncertainty, eq 1 described our data well. The relaxation strength $\Delta\epsilon$ obtained can be used to estimate the value of the dipole moment being involved in the relaxation process. This can be done through the Kirkwood−Fröhlich theory[20−23] from the relation

$$\Delta\epsilon \approx n\frac{\mu^2}{3k_B T\epsilon_0} g_{FK} \qquad (2)$$

where g_{FK} represents the Kirkwood−Fröhlich correlation factor (which in the calculations it was not considered). μ is the dipole moment, n the dipole density, k_B the Boltzmann constant, T the temperature, and ϵ_0 as explained in eq 1.

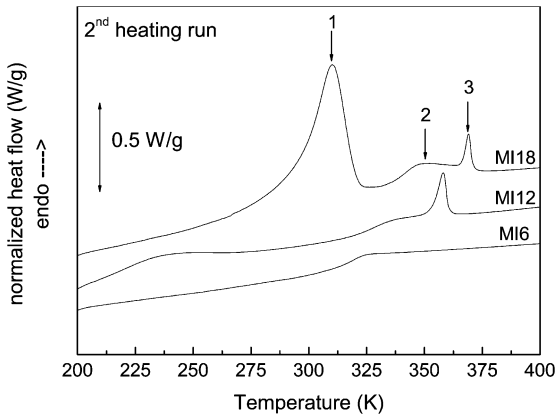

Figure 2. DSC curves of samples MI6, MI12, and MI18 obtained from the second heating at a rate of 20 K/min. Numbers indicate the transition temperatures of the two endothermic transitions (1 and 3) and of the glass transition (2).

Results and Discussion

Differential Scanning Calorimetry. In this paper the transition temperatures and enthalpies of the MI copolymers, summarized in Table 2, will not be discussed in detail. The data obtained by DSC are used as supplemental to dielectric relaxation results. Typical DSC thermograms for MI copolymers MI6, MI12, and MI18 are shown in Figure 2.

From MI1 to MI18 the corresponding glass transition temperature of the MI copolymers decrease, as expected with increasing length of the alkyl side chains (internal plasticization). Also, melting of the side chains is observed for the MI copolymers with longer alkyl side chains. It can be seen that the transition temperatures for the melting of the side chains shift from 236.1 K for MI12 to 310.0 K for MI18. The transition enthalpies are observed to increase accordingly. Wide-angle X-ray diffraction (WAXS) investigation for the MI copolymers revealed backbone-to-backbone distances up to 3.3 nm for MI18 in the solid state,[24] confirming the presence of layered structure. For the MI copolymers MI1−MI6 with shorter alkyl side chains, the melting of the side

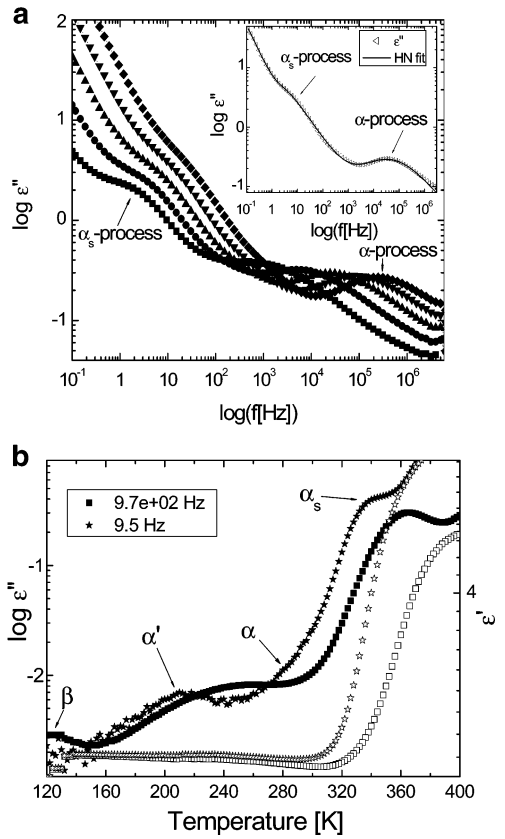

Figure 3. (a) Compound MI3. Dielectric loss vs frequency for different temperatures: 400 K (square), 410 K (circle), 420 K (up-triangle), 430 K (down-triangle), and 440 K (diamonds). The α- and α_s-processes occur on the same frequency window with α_s slower than α. The exponential increase of ϵ'' on the low-frequency side is caused by conductivity contribution. Inset: dielectric loss ϵ'' vs frequency at a temperature of 422 K. The solid line represents the Havriliak and Negami (HN) fit function with parameter $a = 3.032 \times 10^{-10}$ S/m, $s = 0.89$, $\Delta\epsilon_{\alpha_s} = 5.47$, $\tau_{\alpha_s} = 0.057$ s, $\beta_{\alpha_s} = 1$, $\gamma_{\alpha_s} = 0.57$, $\Delta\epsilon_\alpha = 1.22$, $\tau_\alpha = 9.02 \times 10^{-6}$ s, $\beta_\alpha = 0.61$, and $\gamma_\alpha = 0.63$. The error bars are comparable to the size of the symbols, if not indicated otherwise. (b) Compound MI6. Real part (ϵ', open symbols) and imaginary part (ϵ'', solid symbols) of the dielectric function vs temperature at frequencies of 9.5 Hz (star) and 970 Hz (squares). All four relaxation processes, β, α', α, and α_s, are observed in this sample. The α-process is observed as a low-temperature wing at around 280 K in a background of high conductivity.

chains was not detected, implying the apparent absence of side chain crystallization. The described thermal behavior for the glass transition and side chain melting in MI copolymers is similar to MI homopolymers.[25,26] The last point extracted from Table 2 is that a further melting temperature above the glass transition for the MI copolymers possessing side chain melting is observable, which is attributed to order/disorder transition of the material in the bulk. This transition is similar to liquid-crystalline systems[27−30] and is depending on the length of the side chains. The corresponding transition enthalpies are in the same range ($\Delta H = 1.8-3.7$ J/g). For shorter side chains, the order/disorder transition is not observed presumably due to the influence of the helical backbone, which reduces the chances of ordered phases.

Dielectric Spectroscopy. The compounds investigated show different relaxation processes, which are referred here as β, α', α, and α_s according to the sequence of their mean relaxation times. Figure 3a shows

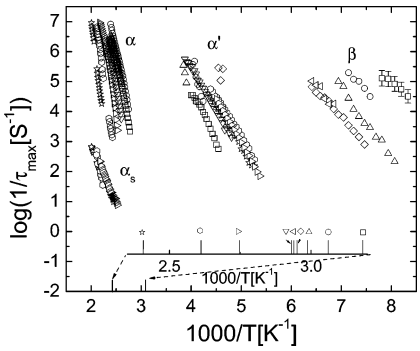

Figure 4. Activation plot showing compounds MI1 (star), MI2 (hexagon), MI3 (right- triangle), MI4 (down-triangle), MI6 (square), MI12 (circle), MI14 (up-triangle), MI16 (diamonds), and MI18 (left-triangle). Inset: corresponding glass transition temperatures (T_g) obtained by DSC measurement. For clarity, error bars are indicated only on one compound, MI6.

Table 3. Dipole Moments and Activation Energies of the *β*-Process for Different CH_2 Units in Alkyl Side Chains of the MI Copolymers[a]

copolymer	CH_2 units	dipole[b] [$\times 10^{-31}$ A s m] (β-relaxation)	dipole [$\times 10^{-30}$A s m] (α'-relaxation)	E_A [kJ/mol]
MI1			1.2 ± 0.1	
MI2	1		1.3 ± 0.1	
MI3	2		1.5 ± 0.1	
MI4	3		1.7 ± 0.1	
MI6	5	8.3 ± 0.1		23.0 ± 4
MI12	11	8.0 ± 0.1		34.0 ± 4
MI14	13	8.3 ± 0.1		45.0 ± 2
MI16	15	9.3 ± 0.1		35.0 ± 2
MI18	17	10.1± 0.1		38.0 ± 6

[a] Dipole moments for the α'-relaxation for copolymers MI1, MI2, MI3, and MI4 are also included. [b] Compared with a molecular calculation of the ethyl radical: 7.7×10^{-31}A s m.

the dielectric loss ϵ'' as a function of frequency for compound MI3 at different temperatures above T_g with the deconvolution of the data (inset) according to eq 1.

From the graph the α_s process is seen to occur at low frequencies. At high temperatures, conductivity contributions due to charge transport mechanisms dominate the ϵ'' spectra at low frequencies. Figure 3b shows the dielectric loss ϵ'' as a function of temperature at 9.5 and 970 Hz for compound MI6.

All four relaxation regions are observed in compound MI6 with the α process appearing as a low-temperature wing. It can also be seen from Figure 3b that β and α' have low dielectric losses and occur at low temperatures where the MI copolymer is in its glassy state. This is the case for all the copolymers studied that show these two processes. Processes α and α_s are independently observable at low frequencies while at high frequencies only one broad peak is observed. The β-relaxation is observed in compounds MI6, MI12, MI14, MI16, and MI18 while α'-relaxation is found to exist in all compounds investigated. The α_s-relaxation has high dielectric strengths for compounds MI1, MI2, and MI3. Figure 4 shows the mean relaxation time ($1/\tau_{max}$) plotted vs inverse temperature for all compounds.

In the following, the different relaxation processes will be discussed.

***β*-Process.** The β-relaxation is observed for all compounds in Table 3, which have their side chain length composed of at least five methylene units as reflected in Figure 4. Its dielectric strength is weak ($\Delta\epsilon \approx 0.03$) compared to that of the α-process ($0.5 < \Delta\epsilon < 2$) and

has an Arrhenius-like temperature dependence of the relaxation times

$$\frac{1}{\tau} = \frac{1}{\tau_0} \exp\left[\frac{-E_A}{k_B T}\right] \quad (3)$$

with E_A denoting the activation energy and τ_0 a preexponential factor. The fact that the β-process makes its appearance as the alkyl side chain becomes longer is evidence that this process is localized in the side chain. It has an Arrhenius-like temperature dependence and is assigned to a libration of the terminal CH_2-CH_3 end group of the side chain.[31] As for the confirmation, the electric dipole moment was estimated using eq 2 (neglecting dipole−dipole interactions), and the values were compared to molecular model calculations (Table 3). Within experimental uncertainty, the dipole moments agree well with calculated values. Furthermore, activation energies obtained by fitting experimental data to eq 3 fall within the range of local processes typically between 20 and 50 kJ/mol[32] (Table 3). It should be mentioned that this relaxation is observed at very low temperatures below the melting temperatures of the side chains. This supports the fact that it is not possible to have large relaxing units of the side chain in the crystalline state, thus the local nature of the process. Interdigitation restrictions also confine relaxation to smaller units of the side chain. The process however shifts slightly to higher temperatures, owing to a slight increase in the length scale of the relaxing units and a slight increase in the dipole density (see Table 3). With increasing temperature, side chain melting occurs, thus introducing mobility to the side chain leading to the α′-process. In the amorphous region, the existence of β-relaxation cannot be excluded although not detectable.

α′-Process. The α′-process is well separated in frequency between the β-relaxation and the dynamic glass transition (α-relaxation). It shows for short alkyl side chains an Arrhenius-type temperature dependence, which changes into a Vogel−Fulcher−Tammann (VFT) behavior for systems with more than five CH_2 units. The latter is typical for the liquid state (above T_g) of glass-forming materials, which is described by the well-known expression[33]

$$\frac{1}{\tau} = \frac{1}{\tau_0} \exp\left[\frac{-DT_0}{T - T_0}\right] \quad (4)$$

where D is the fragility parameter and T_0 is the temperature corresponding to an infinite relaxation time. The dielectric strength of the α′-relaxation is about 0.1, which is more than 3 times stronger compared to the β-relaxation. Both findings (the side chain length dependence and the increased dielectric strength) suggest as molecular assignment of the α′-process a glassy dynamics of the alkyl side chains. This is in accord with similar interpretation for the dynamics of poly(*n*-alkyl methacrylate)s[34−37] or self-assembled alkyl nanodomains.[38] As mentioned earlier, the helical backbone does not seem to favor side chain crystallization of short alkyl chains. As a result, very short chains are able to exhibit fast motions (Arrhenius-type temperature dependence) and long ones are slow (VFT behavior). The relaxation of the long side chains is observed around their melting temperatures.

α-Process. This is the dynamic glass transition process of the copolymers. It is assigned to fluctuations of the succinimide ring.[12,14,39,40] The data have a characteristic temperature dependence according to VFT. The dynamic glass transition temperature is conventionally defined as the temperature where the relaxation time is 100 s.[41,42] By extrapolating the VFT dependence to logarithm $1/\tau_{max} = -2$, the T_g's of the compounds can be deduced. The values obtained are in good agreement with calorimetric data (see Table 2 and Figure 4 with the enlargement of temperature scale by the inset). The α-process shows for the product $T\Delta\epsilon$ (which is constant for a Debye relaxation) an increase with decreasing temperature (Figure 5, open symbols). This reflects the cooperative nature of the dynamic glass transition as observed in low molecular weight systems as well.[43]

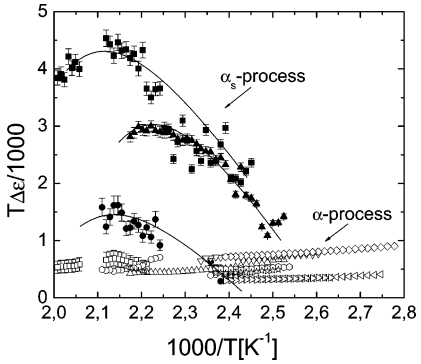

Figure 5. Relaxation strength $T\Delta\epsilon/1000$ vs inverse temperature of α (open symbols) and α_s (closed symbols) for compounds MI1 (square), MI2 (circle), MI3 (up-triangle), MI4 (down-triangle), MI6 (diamonds), MI12 (left-triangle), MI14 (right-triangle), MI16 (hexagonal), and MI18 (star). The lines are guides for the eyes. The relaxation strength for α_s-process goes through a maximum with increasing temperature. For clarity, error bars for the α-process are indicated only on one compound, MI1.

α_s-Process. This relaxation is about 4 decades in frequency slower than that of the glass transition temperature. It is not affected by the length of the side chains. Its dielectric strength (Figure 5, closed symbols) is about 3 times stronger than that of the dynamic glass transition. This proves that the fluctuating units involved must correspond to an underlying molecular superstructure of about 2−3 succinimide rings. This interpretation is in full accord with structural studies[1,44,45] of maleimides in which the helical structure of a 3_1-helix conformation is reported. Additional NMR studies[40,46] and molecular modeling calculations (Figure 6 and Supporting Information) of maleimides support the helical main chain conformation in alternating maleimides surrounded by partly/completely extended aliphatic side chains. The peculiar maximum in the $T\Delta\epsilon$ vs $1000/T$ is interpreted in the following way: with increasing temperature, the mobility of the maleimide rings increases, enabling the system to develop a supermolecular configuration. But this effect is counterbalanced if thermal fluctuations become dominating compared to the intermolecular interactions. The decrease in the dielectric strength of α_s-process with increasing side chain length may be explained in terms decoupling of side chain effects from main chain motions. In Figure 6, the different molecular and supramolecular fluctuations are schematically represented.

Conclusion

The molecular dynamics in several poly(ethene-*alt*-*N*-alkylmaleimide)s was studied by broadband dielectric

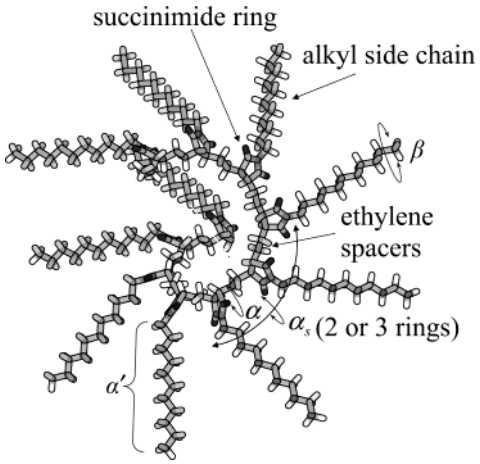

Figure 6. Schematic representation of the relaxations in poly(ethene-*alt*-*N*-alkylmaleimide), using 10 repeating units with the trans configuration of the succinimide rings (based on a threo−diisotactic sequence derived from results in ref 46). The view is on the direction of the main chain. The α and α_s-processes are main chain motions involving the succinimide rings. α′ is a relaxation of the side chain while α and α_s are in-plane motions with α_s originating from an ensemble of about 2−3 rings. The *β*-process is a librational motion of the CH_2-CH_3 group at the terminal position of the alkyl side chain.

spectroscopy. Four dielectrically active relaxations are observed: the *β*-relaxation attributed to librational motions at the terminal position of the alkyl side chain, the α′-process which is assigned to the glass transition relaxation of the side chain, the α-process designated to the dynamic glass transition, and finally the α_s-relaxation reflecting a cooperative motion involving 2−3 succinimide rings. Glass transition temperatures determined dielectrically agree well with calorimetric measured values. A model was proposed to explain the extraordinary slow relaxation of maleimide rings in an underlying helical superstructure.

Acknowledgment. The financial support for J. Tsuwi by the German Academic Exchange Service (DAAD) is acknowledged. We thank Mrs. L. Häussler for carrying out the DSC measurements.

Supporting Information Available: Additional molecular modeling calculations of maleimides. This material is available free of charge via the Internet at http://pubs.acs.org.

References and Notes

(1) Cubbon, R. C. P. *J. Polym. Sci., Part C* **1967**, *16*, 387.
(2) (a) Verbiest, T.; Samyn, C.; van Beylen, M.; Persoons, A. *Macromol. Rapid Commun.* **1998**, *19*, 349. (b) Gangadhara, S.; Ponrathnam, S.; Noel, C.; Reyx, D.; Kajzar, F. *J. Polym. Sci., Part A: Polym. Chem.* **1999**, *37*, 513.
(3) (a) Chiang, W.-Y.; Lu, J.-Y. *Macromol. Chem. Phys.* **1994**, *195*, 591. (b) Chae, K. H.; Gwark, J. C.; Chang, T. *Macromol. Rapid Commun.* **1998**, *19*, 349.
(4) Kwok, D. Y.; Li, A.; Lam, C. N. C.; Wu, R.; Zschoche, S.; Pöschel, K.; Gietzelt, T.; Grundke, K.; Jacobsch, H.-J.; Neumann, A. W. *Macromol. Chem. Phys.* **1999**, *200*, 1121.
(5) (a) del Rio, O. I.; Kwok, D. Y.; Wu, R.; Alvarez, J. M.; Neumann, A. W. *Colloids Surf. A: Physiochem. Eng. Aspects* **1998**, *143*, 197. (b) Grundke, K.; Zschoche, S.; Pöschel, K.; Gietzelt, T.; Michel, S.; Friedel, P.; Jehnichen, D.; Neumann, A. W. *Macromolecules* **2001**, *34*, 6768.
(6) Lange, R. F. M.; Meijer, E. W. *Macromolecules* **1995**, *28*, 6768.
(7) (a) Gouzy, M. F.; Sperling, C.; Streller, U.; Salchert, K.; Böhme, F.; Voit, B.; Werner, C. *Polym. Prepr.* **2002**, *43*, 695. (b) Pompe, T.; Zschoche, S.; Salchert, K.; Herold, N.; Werner, C. *Biomacromolecules* **2003**, *4*, 1072.
(8) Yan, H.; Zhu, X. *J. Appl. Polym. Sci.* **1999**, *74*, 97.
(9) Fleš, D. D.; Golija, G.; Hace, D.; Vukovic, R.; Fleš, D. *Polym. Bull. (Berlin)* **1994**, *33*, 425.
(10) (a) Hendlinger, P.; Laschewsky, A.; Bertrand, P.; Delcorte, A.; Legras, R.; Nysten, B.; Möbius, D. *Langmuir* **1997**, *13*, 310. (b) Jeong, H.; Lee, B.-J.; Cho, W. J.; Ha, C.-S. *Polymer* **2000**, *41*, 5525.
(11) Appelhans, D.; Wang, Z. G.; Zschoche, S.; Zhuang, R.-C.; Häussler, L.; Friedel, P.; Simon, F.; Jehnichen, D.; Grundke, K.; Eichhorn, K.-J. *Macromolecules*, submitted for publication.
(12) Block, H.; Grooves, R.; Walker, S. M. *Polymer* **1972**, *13*, 527.
(13) Colomer, R. F.; Duerìas, J. M. M.; Ribelles, J. L. G.; Barrales-Rienda, J. M.; Bautista de Ojeda, J. M. *Macromolecules* **1993**, *26*, 155.
(14) Block, H.; Lord, P. W.; Walker, S. M. *Polymer* **1975**, *16*, 739.
(15) Bauer, B.; et al. *SuSE Linux 8.2 Manual*, ISBN 3-930-419-67-X, 1998.
(16) Schmidt, M. W.; Baldridge, K. K.; Boatz, J. A.; Elbert, S. T.; Gordon, M. S.; Jensen, J. H.; Koseki, S.; Matsunaga, N.; Nguyen, K. A.; Su, S.; Windus, T. L.; Dupuis, M.; Montgomery, J. A. *J. Comput. Chem.* **1993**, *14*, 1347.
(17) Friedel, P. RESMAIN, Program for building linear and hyperbranched polymers with optional parameters choosing constitutional and conformational statistics. Institute of Polymer Research Dresden, 1998−2003.
(18) Kremer, F.; Schönhals, A. In *Broadband Dielectric Spectroscopy*; Kremer, F., Schönhals, A., Eds.; Springer: Berlin, 2003; Chapter 2.
(19) Havriliak, S.; Negami, S. *J. Polym. Sci.* **1966**, *C14*, 99.
(20) Böttcher, C. J. F. *Theory of Electric Polarization*, 2nd ed.; Elsevier: Amsterdam, 1973: Vol. I, p 181.
(21) Fröhlich, H. *Theory of Dielectrics*; Oxford University Press: London, 1958.
(22) Onsager, L. *J. Am. Chem. Soc.* **1938**, *58*, 1486.
(23) Kirkwood, J. G. *J. Chem. Phys. Soc.* **1939**, *7*, 911.
(24) Appelhans, D.; Wang, Z. G.; Zschoche, S.; Zhuang, R.-C.; Häussler, L.; Friedel, P.; Simon, F.; Jehnichen, D.; Komber, H.; Grundke, K.; Eichhorn, K.-J. *Macromolecules*, submitted for publication.
(25) Barrales-Rienda, J. M.; Fernandez-Martin, F.; Galicia, C. R.; Chaves, M. S. *Makromol. Chem.* **1983**, *184*, 2643.
(26) Barrales-Rienda, J. M.; Gonzales Ramos, J.; Chaves, M. S. *Br. Polym. J.* **1977**, *184*, 2643.
(27) Kinning, D. J. *J. Adhes.* **1997**, *60*, 249.
(28) Platé, N. A.; Shibaev, V. P. *J. Polym. Sci., Macromol. Rev.* **1974**, *8*, 177.
(29) Gottwald, A.; Pospiech, D.; Jehnichen, D.; Häussler, L.; Friedel, P.; Pionteck, J.; Stamm, M.; Floudas, G. *Macromol. Chem. Phys.* **2002**, *203*, 854.
(30) Corpart. J. M.; Girault, S.; Juhué D. *Langmuir* **2001**, *17*, 7237.
(31) Groothues, H.; Kremer, F.; Pelsnivy, T.; Ringsdorf, H. *Macromol. Chem. Phys.* **1996**, *197*, 3881.
(32) Schönhals, A. In *Broadband Dielectric Spectroscopy*; Kremer, F., Schönhals, A., Eds.; Springer: Berlin, 2003; p 243.
(33) Vogel, H. *Phys. Z.* **1921**, *22*, 645. Fulcher, G. S. *J. Am. Chem. Soc.* **1925**, *8*, 339. Tammann, G.; Hesse, G. *Anorg. Allg. Chem.* **1926**, *156*, 245.
(34) Garwe, F.; Schönhals, A.; Lockwenz, H.; Beiner, M.; Schröter, K.; Donth, E. *Macromolecules* **1996**, *29*, 247.
(35) Floudas, G.; Štepánek, P. *Macromolecules* **1998**, *31*, 6951.
(36) Beiner, M.; Schröter, K.; Hempel, E.; Reissig, S.; Donth, E. *Macromolecules* **1999**, *32*, 6278.
(37) Gaur, U.; Wunderlich, B. *Macromolecules* **1980**, *13*, 445.
(38) (a) Beiner, M.; Huth, H. *Nature Mater. Lett.* **2003**, *2*, 595. (b) Hiller, S.; Pascui, O.; Budde, H.; Kabisch, O.; Reichert, D.; Beiner, M *New J. Phys.* **2004**, *6*, 10.
(39) Bailey, J.; Walker, S. M. *Polymer* **1972**, *13*, 561.
(40) Block, H.; Evans, D.; Walker, S. M. *Polymer* **1977**, *18*, 786.
(41) Donth, E. *Glassübergang*; Academie Verlag: Berlin, 1981.
(42) Angell, C. A. *Science* **1995**, *267*, 1924.
(43) Schönhals, A.; Kremer, F.; Stickel, F. *Phys. Rev. Lett.* **1993**, *71*, 4096.
(44) Baltá-Calleja, F. J.; Ramos, J. G.; Barrales-Rienda, J. M. *Kolloid Z. Z. Polym.* **1972**, *250*, 474.
(45) Percec, V.; Schlueter, D.; Ronda, J. C.; Johansson, G.; Ungar, G.; Zhou, J. P. *Macromolecules* **1996**, *29*, 1464.
(46) Komber, H. *Macromol. Chem. Phys.* **1995**, *196*, 669.

MA049370O